Localization in 2D PBR with Multiple Transmitters of Opportunity: A Constrained Least Squares Approach

Augusto Aubry, *Senior Member IEEE*, Vincenzo Carotenuto, *Senior Member IEEE*, Antonio De Maio, *Fellow, IEEE*, and Luca Pallotta, *Senior Member IEEE*

***Abstract*—A new algorithm for Passive Bistatic Radar (PBR) localization exploiting multiple illuminators of opportunity is proposed. To capitalize a-priori information on the receiving antenna main-lobe extent, specific constraints are forced to the target localization process. At the estimator design process the elliptic positioning problem is formulated according to the constrained Least Squares (LS) framework. Hence, the resulting non-convex optimization problem is globally solved providing a closed-form estimate to the target Cartesian coordinates. At the analysis level, the performance of the new estimator is assessed in terms of Root Mean Square Error (RMSE) behavior. The results highlight that interesting MSE improvements with respect to some counterparts available in the open literature can be achieved especially at low Signal to Noise Ratio (SNR) values.**

***Index Terms*—Passive Bistatic Radar (PBR), Multiple Transmitter of Opportunity, Elliptic Localization, Range Measurements.**

I. Introduction

In modern battlefield and civilian scenarios it is becoming more and more valuable the development of passive surveillance systems capable of detecting, localizing, and tracking hostile and/or unknown targets (also of stealth type), while keeping covertness, a wide coverage range, and an overall low cost [1]–[4]. In this context, Passive Bistatic Radar (PBR), also known as "Green Radar" [5], is widely recognized among the most promising and effective passive sensing technologies [5], [6]. PBR based localization is accomplished using bistatic target range measurements obtained collecting the target echoes resulting from the signals transmitted by one/multiple illuminators of opportunity [6], [7, Chap. 11]. To this end, PBR receivers are equipped with two receiving channels per transmitter of oppurtunity: one is used to acquire the direct path signal from the selected emitter, the other to gather the induced echoes. Each pair of measurements allows to localize the target over an ellipsoid (ellipse in a 2D geometry) and the intersection of multiple ellipsoids due to different illuminator-passive receiver pairs paves the way for target positioning [6], [7]. As a result, PBR problem falls within the elliptical range sum class [8]–[10] where several strategies have been developed in the open literature to provide reliable target position estimate. Moreover, many other research papers dealing with the passive localization together with its fundamental limits can be found in the open literature [11]–[13].

In [14] an iterative algorithm for the synchronous elliptic localization problem (i.e., receiver and transmitters are assumed synchronized) is provided assuming the knowledge of the measurement accuracies. In [15], the authors exploit the information provided by asynchronous absolute range measurements to improve the position estimation accuracy in an elliptical measurement system. Assuming a multistatic configuration, two-Dimensional (2D) target localization is addressed in [16] exploiting the properties of signals scattered by helicopter blades; in [17], resorting to solutions techniques developed in the context of Time Difference of Arrival (TDOA) systems, two closed-form localization methods compatible with real-time applications are proposed and compared for passive systems with one receiver and multiple transmitters. Some interesting theoretical results on the performance of PBR systems are provided in [18] where the Cramer Rao Lower Bound (CRLB) on the bistatic range and Doppler frequency estimates with missing observations is derived for a multistatic radar networks. Additional applications of elliptic positioning within the radar signal processing context can be found for instance in [19]–[21]. Furthermore, in [22] the authors derive an algebraic solution for moving target localization in multi-transmitter multi-receiver passive radar systems using bistatic range and range rate measurements. In [23], [24], the hybrid passive radar concept is introduced where the joint exploitation of the signals broadcasted by the same transmitter at different carrier frequencies is considered to increase the system reliability. In [25] an advanced PBR-based system is proposed, where active transmitters (to be utilized in case of absence/failure of the transmitters of opportunity or in addition to them) is included in the sensing network. By doing so, performance improvement as well as a more robust and reliable behavior are guaranteed to the surveillance system. Strategies able to strenghten system performance exploiting different transmitter of opportunity (such as FM-radio, DVB-T) to promote waveform diversity are also developed in [26], [27]. Finally, some attempts to exploit the PBR paradigm have been pursued both in the context of Synthetic Aperture Radar (SAR) [28]–[30] and tracking systems [31]–[33].

This paper proposes an innovative approach for elliptic lo-

Augusto Aubry, Vincenzo Carotenuto, and Antonio De Maio are with Università degli Studi di Napoli "Federico II", DIETI, Via Claudio 21, I-80125 Napoli, Italy. E-mail: augusto.aubry@unina.it, vincenzo.carotenuto@unina.it, ademaio@unina.it.

Luca Pallotta was with CNIT udr Università "Federico II", via Claudio 21, I-80125 Napoli, Italy (he is now with the Department of Engineering, University of Roma Tre, via Vito Volterra 62, 00146 Rome, Italy, E-mail: luca.pallotta@uniroma3.it.)

cation with reference to a 2D PBR receiver exploiting multiple transmitters of opportunity. At the design level, it is assumed that the receiving antenna has a 2D directional beampattern and specific constraints to account for its main-beam size are enforced to the target localization process. The motivation of the present study relies on the observation that many PBR systems available on the market employ a circular array antenna which scans in azimuth with a given main-lobe size (quantified by the 3-dB angular extent). These systems often work in a low Signal to Noise Ratio (SNR) regime (consider for instance the localization of Unmanned Aerial Vehicles (UAV) with very low radar cross section) and it seems thus natural and of practical importance to boost the performance exploiting the receive main-lobe extent information within the localization process. Therefore, positioning is formulated as a constrained Least Squares (LS) estimation whose optimal solution provides the Cartesian coordinates of the target. It is proved that the resulting non-convex optimization problem can be efficiently solved resorting to the theory of Generalized Trust Region Subproblems (GTRSs) [34], already exploited for the case of hyperbolic location in [35], and a closed-form target location estimate is provided. From the optimization theory point of view this is the main achievement of the present paper. Along the analysis, the performance of the proposed algorithm is assessed in comparison with the unconstrained LS positioning solution, the Two-Step Estimation (TSE) procedure [14] which estimates the target position via an iterative algorithm, and the CRLB on the target Cartesian coordinates that provides a benchmark on the achievable estimation accuracy.

The paper is organized as follows. Section II introduces the system model and defines the constraints due to receive antenna main-beam. Section III formulates the constrained LS estimation approach and presents the technique to obtain a closed-form solution to the problem at hand. In Section IV, some efficient algorithms available in open literature to estimate target position without accounting for receive antenna main-beam induced constraints are described. Section V is devoted to the performance analysis of the proposed PBR localization algorithm together with the discussion of the obtained results. Finally, Section VI draws some conclusions and highlights possible future research avenues.

A. Notation

We adopt the notation of using boldface for vectors $\boldsymbol{a}$ (lower case), and matrices $\boldsymbol{A}$ (upper case). The n-th element of $\boldsymbol{a}$ and the (m,l)-th entry of $\boldsymbol{A}$ are respectively denoted by a_n and $\boldsymbol{A}_{m,n}$. The symbols $(\cdot)^T$ indicates the transpose operator. $\boldsymbol{A}^\dagger$ represents the Moore-Penrose inverse of the matrix $\boldsymbol{A}$. $\boldsymbol{I}$ and $\boldsymbol{0}$ denote respectively the identity matrix and the matrix with zero entries (their size is determined from the context). $\mathbb{R}^N$, $\mathbb{R}^{N,M}$, and $\mathbb{S}^N$ are respectively the sets of N-dimensional vectors of real numbers, of $N\times M$ real matrices, and of $N\times N$ symmetric matrices. $\mathbf{diag}\,(\boldsymbol{a})$ indicates the diagonal matrix whose i-th diagonal element is the i-th entry of $\boldsymbol{a}$. The curled inequality symbol $\succeq$ (and its strict form $\succ$) is used to indicate generalized matrix inequality: for any $\boldsymbol{A}\in\mathbb{S}^N$, $\boldsymbol{A}\succeq\boldsymbol{0}$ means that $\boldsymbol{A}$ is a positive semi-definite matrix ($\boldsymbol{A}\succ\boldsymbol{0}$ for positive definiteness). $\lambda_1(\boldsymbol{X}),\lambda_2(\boldsymbol{X}),\ldots,\lambda_N(\boldsymbol{X})$, with $\lambda_1(\boldsymbol{X})\geq\lambda_2(\boldsymbol{X})\geq\ldots\geq\lambda_N(\boldsymbol{X})$, denote the eigenvalues of $\boldsymbol{X}\in\mathbb{S}^N$, arranged in decreasing order. Furthermore, given $\boldsymbol{B}\succ\boldsymbol{0}$ and $\boldsymbol{A}\in\mathbb{S}^N$, the generalized eigenvalues of the matrix pair $(\boldsymbol{A},\boldsymbol{B})$ are given by $\lambda_i(\boldsymbol{A},\boldsymbol{B})=\lambda_i(\boldsymbol{B}^{-1/2}\boldsymbol{A}\boldsymbol{B}^{-1/2})$, $i=1,\ldots,N$. The Euclidean norm of the vector $\boldsymbol{x}$ is denoted by $\|\boldsymbol{x}\|$. The letter i often serves as index. Furthermore, given a real scalar function $f(\boldsymbol{x})$, $\boldsymbol{x}\in\mathbb{R}^N$, $\nabla f(\boldsymbol{x})=\left[\frac{\partial f(\boldsymbol{x})}{\partial x_1},\ldots,\frac{\partial f(\boldsymbol{x})}{\partial x_N}\right]^T\in\mathbb{R}^N$ represents the gradient vector of the function $f(\boldsymbol{y})$ evaluated at $\boldsymbol{y}=\boldsymbol{x}$. $\mathbb{E}\left[\cdot\right]$ indicates the statistical expectation and for any optimization Problem $\mathcal{P}$, $v(\mathcal{P})$ represents its optimal value.

II. System Model

Consider a 2D passive bistatic radar exploiting multiple transmitters of opportunity, as illustrated in Figure 1. Then, denote by:

- $(x_p,y_p)\in\mathbb{R}^2$ the target position;
- $(x_0,y_0)\in\mathbb{R}^2$ the receiver position (without loss of generality, it is assumed to coincide with the reference system origin, i.e., $(x_0,y_0)=(0,0)$);
- $(x_{t_i},y_{t_i})\in\mathbb{R}^2$ the position of the i-th transmitter of opportunity, $i=1,\ldots,N$;
- $L_i\in\mathbb{R}$ the distance between the i-th transmitter and the receiver, namely, $\sqrt{(x_{t_i}-x_0)^2+(y_{t_i}-y_0)^2}$, $i=1,\ldots,N$.
- $\boldsymbol{p}=[x_p,y_p]^T$ the target position vector.

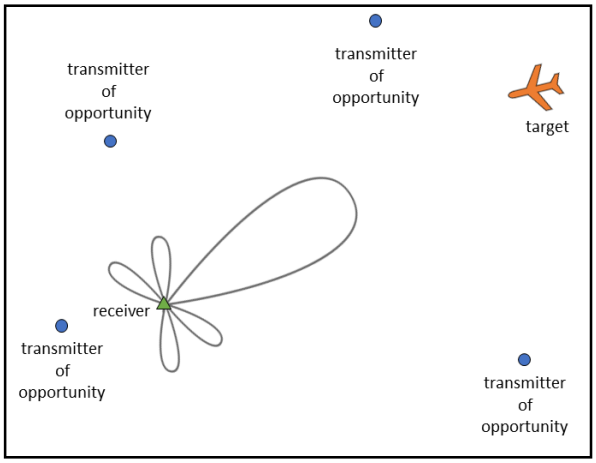

Fig. 1. Notional representation of a typical PBR system including one receiver and multiple transmitters of opportunity for a 2D sensing geometry.

At the receiver side, after the classic PBR cross-correlation based processing, the following N delay/range measurements are available

$$\tau_i=\tilde{\tau}_i+n_i,\ i=1,\ldots,N, \tag{1}$$

where, for $i=1,\ldots,N$,

$$\tilde{\tau}_i=\frac{1}{c}\left(\|\boldsymbol{p}\|+\sqrt{(x_p-x_{t_i})^2+(y_p-y_{t_i})^2}-L_i\right), \tag{2}$$

with c the speed of light and $n_1,\ldots,n_N$ statistically independent zero-mean (usually assumed Gaussian distributed, even if

this assumption is not mandatory for the present paper) random variables with variance $\sigma_1^2, \ldots, \sigma_N^2$. In particular,

$$\sigma_i = \frac{1}{B_i\sqrt{2\mathrm{SNR}_i}}, \; i = 1, \ldots, N, \tag{3}$$

where B_i is the frequency bandwidth of the i-th signal of opportunity and SNR_i is the SNR of the i-th bistatic pair (i.e., receiver/i-th transmitter of opportunity) evaluated according to the bistatic radar range equation [18], [36]. Evidently, due to both spatial (geometric configuration) and spectral (signal bandwidth) diversity of the transmitters of opportunity, the amount of noise depends on the specific bistatic pair.

Now, elaborating on (2), it is possible to get an equivalent form which is fundamental for the proposed estimation algorithm. To this end, denoting by

$$b_i = \tilde{\tau}_i c + L_i \quad i = 1, \ldots, N\,, \tag{4}$$

equation (2) can be recast as[1]

$$b_i - \sqrt{x_p^2 + y_p^2} = \sqrt{(x_p - x_{t_i})^2 + (y_p - y_{t_i})^2}\,, i = 1, \ldots, N, \tag{5}$$

or equivalently as

$$\begin{cases} b_i^2 + r^2 - 2b_i r = r^2 + r_i^2 - 2x_{t_i}x_p - 2y_{t_i}y_p, \\ r \leq b_i \qquad\qquad\qquad\qquad\qquad i = 1, \ldots, N, \\ r = \sqrt{x_p^2 + y_p^2} \end{cases} \tag{6}$$

with $r_i = \sqrt{x_{t_i}^2 + y_{t_i}^2}$, $i = 1, \ldots, N$. All the relationships described in (6) can be also framed in a more compact matrix form

$$\begin{cases} \boldsymbol{A}\bar{\boldsymbol{p}} - \boldsymbol{g} = \boldsymbol{0} \\ \bar{\boldsymbol{p}}^T \boldsymbol{B}\bar{\boldsymbol{p}} = 0 \\ \bar{p}_3 \leq b_i, \; i = 1, \ldots, N \end{cases} \tag{7}$$

where

- $\bar{\boldsymbol{p}} = [\boldsymbol{p}^T, r]^T \in \mathbb{R}^3$;
- $\boldsymbol{A}^T = [\boldsymbol{a}_1, \boldsymbol{a}_2, \ldots, \boldsymbol{a}_N] \in \mathbb{R}^{3,N}$, with

$$\boldsymbol{a}_i = [-2x_{t_i}, -2y_{t_i}, 2b_i]^T \in \mathbb{R}^3\,, \; i = 1, \ldots, N \tag{8}$$

- $\boldsymbol{g} = [b_1^2 - r_1^2, b_2^2 - r_2^2, \ldots, b_N^2 - r_N^2]^T \in \mathbb{R}^N$;
- $\boldsymbol{B} = \mathbf{diag}\,\{[1, 1, -1]\} \in \mathbb{R}^{3,3}$.

A. Receiver Antenna Main-Lobe Extent Constraint

To perform the search process, conventional 2D PBR systems employ a scanning antenna (in the azimuth domain) characterized by a specific beampattern and in particular a given main-lobe width. In this subsection, some constraints able to capitalize such a-priori information are formalized with the goal of improving target localization reliability. To this end, let us denote by (see Figure 2):

- $\bar{\theta}$ the receiving (half-side) antenna beamwidth (with respect to the boresight), with $0 \leq \bar{\theta} < \pi/2$;
- $\theta \in \,]-\pi, \pi[$ the squint angle of the antenna boresight with respect to the x-axis;
- For $(x_p, y_p) \neq (0, 0)$, $\theta_p = \mathrm{atan2}(y_p, x_p)$ the target angle of arrival, where $\mathrm{atan2}(\cdot)$ is the four-quadrants inverse tangent.

Suppose, now, that the target is within the receiving antenna main-beam (as pictorially illustrated in Figure 2), i.e., that

$$\theta - \bar{\theta} \leq \theta_p \leq \theta + \bar{\theta} \tag{9}$$

or equivalently

$$-\bar{\theta} \leq \theta_p - \theta \leq \bar{\theta}. \tag{10}$$

Otherwise stated, it is assumed that the detector performs correctly its task, i.e., the target triggering the detection resides in the antenna main-beam[2].

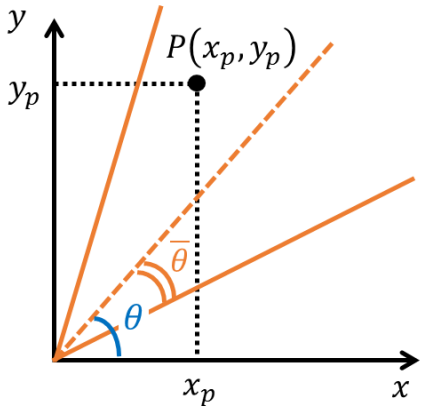

Fig. 2. Representation of the angles involved in the localization process, i.e., antenna main-beam and boresight squint angle.

Equation (10) coupled with the assumption $0 \leq \bar{\theta} < \frac{\pi}{2}$ can be equivalently rewritten as

$$-\tan\bar{\theta} \leq \tan(\theta_p - \theta) \leq \tan\bar{\theta} \tag{11}$$

and

$$|\theta_p - \theta| < \frac{\pi}{2}. \tag{12}$$

Now, the following relationships on the tangent function hold

$$\begin{aligned} \tan(\theta_p - \theta) &= \frac{\sin(\theta_p - \theta)}{\cos(\theta_p - \theta)} \\ &= \frac{\sin(\theta_p)\cos(\theta) - \cos(\theta_p)\sin(\theta)}{\cos(\theta_p)\cos(\theta) + \sin(\theta_p)\sin(\theta)} \\ &= \frac{y_p\cos\theta - x_p\sin\theta}{x_p\cos\theta + y_p\sin\theta}, \end{aligned} \tag{13}$$

where the last equality stems from $\sin\theta_p = y_p/\sqrt{x_p^2 + y_p^2}$ and $\cos\theta_p = x_p/\sqrt{x_p^2 + y_p^2}$.

[1]The idea of squaring and introducing the auxiliary variable r is well known since [37] (for the range difference case) and highlighted in [8] (for the range sum case).

[2]In the presence of intentional sidelobe interference, advanced radar detectors equipped for instance with a Sidelobe Blanking (SLB) architecture [38] could be employed.

Exploiting (13), (11) can be written in a more useful form i.e. as

$$-\tan\bar{\theta} \leq \frac{y_p\cos\theta - x_p\sin\theta}{x_p\cos\theta + y_p\sin\theta} \leq \tan\bar{\theta}. \tag{14}$$

Let us now manipulate the previous inequalities introducing a new reference system, say (x_1, y_1), obtained rotating the actual one (i.e., the (x, y)-coordinates system) such that the x_1-axis is aligned with the receiving antenna boresight. This concept is graphically illustrated in Figure 3. Precisely, denoting by $\bar{\boldsymbol{R}}(\theta)$ the rotation matrix of an angle θ clockwise, i.e.,

$$\bar{\boldsymbol{R}}(\theta) = \begin{bmatrix} \cos\theta & \sin\theta \\ -\sin\theta & \cos\theta \end{bmatrix}, \tag{15}$$

the new (x_1, y_1)-coordinates system is related to the previous (x, y)-coordinates system by means of the following transformation

$$\begin{bmatrix} x_1 \\ y_1 \end{bmatrix} = \bar{\boldsymbol{R}}(\theta)\begin{bmatrix} x \\ y \end{bmatrix} = \begin{bmatrix} x\cos\theta + y\sin\theta \\ -x\sin\theta + y\cos\theta \end{bmatrix}. \tag{16}$$

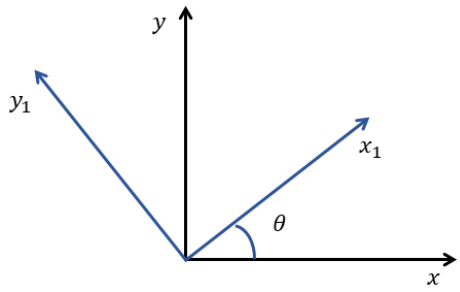

Fig. 3. Reference system with x_1-axis coinciding with the antenna boresight.

Consequently, (14) becomes

$$-\tan\bar{\theta} \leq \frac{y_{1p}}{x_{1p}} \leq \tan\bar{\theta}, \tag{17}$$

where x_{1p} and y_{1p} are the new coordinates associated with x_p and y_p.

From the relationship

$$|\text{atan2}\,(y_{1p}, x_{1p})| = |\text{atan2}\,(y_p, x_p) - \theta| < \frac{\pi}{2}, \tag{18}$$

it directly follows that $x_{1p} > 0$. Hence, the additional constraints to consider at the estimator design development as induced by the antenna beamwidth are given by

$$\begin{cases} -x_{1p}\tan\bar{\theta} \leq y_{1p} \leq x_{1p}\tan\bar{\theta} \\ x_{1p} > 0 \end{cases}. \tag{19}$$

Finally, to take in account also the point with coordinates $(x_{1p}, y_{1p}) = (0, 0)$ and letting $\gamma = \tan\bar{\theta}$, the constraints in (19) can be expressed as

$$\begin{cases} -x_{1p}\gamma \leq y_{1p} \leq x_{1p}\gamma \\ x_{1p} \geq 0 \\ \begin{bmatrix} x_{1p} \\ y_{1p} \end{bmatrix} = \bar{\boldsymbol{R}}(\theta)\begin{bmatrix} x_p \\ y_p \end{bmatrix} \end{cases}. \tag{20}$$

III. Problem Formulation

Starting from (7), it can be observed that the first equation holds only approximately in practical situations due to measurement errors (1). A viable mean to overcome this shortcoming is to resort to the constrained LS framework and formalize the estimation problem as

$$\begin{cases} \min\limits_{\bar{\boldsymbol{p}}} & \|\boldsymbol{A}\bar{\boldsymbol{p}} - \boldsymbol{g}\|^2 \\ \text{s.t.} & \bar{\boldsymbol{p}}^T\boldsymbol{B}\bar{\boldsymbol{p}} = 0 \\ & 0 \leq \bar{p}_3 \leq b \end{cases} \tag{21}$$

with $b = \min\limits_{i=1,\ldots,N} b_i$. Notice that, with a slight abuse of notation, the model parameters in (21), i.e., $\boldsymbol{A}$, $\boldsymbol{g}$, and b, are computed exploiting the actual measurements τ_i, $i = 1, \ldots, N$, in place of $\tilde{\tau}_i$, $i = 1, \ldots, N$.

In the current form the considered estimation problem (21) does not account for the receive antenna main-beam constraints introduced in II-A. Thus, to proceed further, let us introduce the target position vector in the rotated (x_1, y_1)-coordinates reference system, indicated in the following as $\tilde{\boldsymbol{p}}$. Precisely, the position vector in the rotated coordinate system is given by $\tilde{\boldsymbol{p}} = \boldsymbol{U}^T\bar{\boldsymbol{p}}$, where

$$\boldsymbol{U} = \begin{bmatrix} \bar{\boldsymbol{R}}(\theta)^T & 0 \\ 0 & 1 \end{bmatrix} \tag{22}$$

with $\boldsymbol{U}^T\boldsymbol{U} = \boldsymbol{I}$. As a consequence, elliptic localization problem with the addition of the main-lobe extent constraints (20), is formulated as

$$\begin{cases} \min\limits_{\tilde{\boldsymbol{p}}} & \|\boldsymbol{A}\boldsymbol{U}\tilde{\boldsymbol{p}} - \boldsymbol{g}\|^2 \\ \text{s.t.} & \tilde{\boldsymbol{p}}^T\boldsymbol{U}^T\boldsymbol{B}\boldsymbol{U}\tilde{\boldsymbol{p}} = 0 \\ & 0 \leq \tilde{p}_3 \leq b \\ & -\tilde{p}_1\gamma \leq \tilde{p}_2 \leq \tilde{p}_1\gamma \\ & \tilde{p}_1 \geq 0 \end{cases} \tag{23}$$

Finally, introducing $\tilde{\boldsymbol{A}} = \boldsymbol{A}\boldsymbol{U}$ and since $\boldsymbol{U}^T\boldsymbol{B}\boldsymbol{U} = \boldsymbol{B}$, (23) can be recast as

$$\mathcal{P}\begin{cases} \min\limits_{\tilde{\boldsymbol{p}}} \left\|\tilde{\boldsymbol{A}}\tilde{\boldsymbol{p}} - \boldsymbol{g}\right\|^2 & \\ \text{s.t. } \tilde{\boldsymbol{p}}^T\boldsymbol{B}\tilde{\boldsymbol{p}} = 0 & \text{(24a)} \\ \quad 0 \leq \tilde{p}_3 \leq b & \text{(24b)} \\ \quad -\tilde{p}_1\gamma \leq \tilde{p}_2 \leq \tilde{p}_1\gamma & \text{(24c)} \\ \quad \tilde{p}_1 \geq 0 & \text{(24d)} \end{cases}$$

Problem $\mathcal{P}$ is a non-convex optimization problem apparently difficult to solve. However, leveraging the special structure of the objective function/constraints and resorting to the theory of GTRSs [34], a closed-form optimal solution to $\mathcal{P}$ is now derived. A first step toward this goal is provided by the following lemma

Lemma 3.1: Any feasible point $\boldsymbol{x} \neq (0, 0, 0)$ is regular for the optimization Problem $\mathcal{P}$.

Proof: See Appendix A ∎

The following proposition establishes a procedure leading to a closed-form global optimal solution of the constrained

estimation problem $\mathcal{P}$. This represents the main technical contribution of the present paper from an optimization theory point of view.

Proposition 3.2: An optimal solution to $\mathcal{P}$ belongs to the following finite set of feasible points (whose cardinality is at most thirteen):

1) $\bar{\boldsymbol{x}}_0^\star = \mathbf{0}$.
2) $\bar{\boldsymbol{x}}^\star(\eta_h) = \left(\tilde{\boldsymbol{A}}^T\tilde{\boldsymbol{A}} + \eta_h \boldsymbol{B}\right)^{-1}\tilde{\boldsymbol{A}}^T\boldsymbol{g}$, where η_h, $h = 1,\ldots,N_r$ ($N_r \leq 4$), are the roots of the fourth order equation
$$\bar{\boldsymbol{x}}^\star(\eta)^T\boldsymbol{B}\bar{\boldsymbol{x}}^\star(\eta) = 0 \tag{25}$$
with
$$\eta \in \left(-\frac{1}{\lambda_2\left(\boldsymbol{B},\tilde{\boldsymbol{A}}^T\tilde{\boldsymbol{A}}\right)},+\infty\right) - \left\{-\frac{1}{\lambda_1\left(\boldsymbol{B},\tilde{\boldsymbol{A}}^T\tilde{\boldsymbol{A}}\right)},-\frac{1}{\lambda_3\left(\boldsymbol{B},\tilde{\boldsymbol{A}}^T\tilde{\boldsymbol{A}}\right)}\right\} \tag{26}$$
such that
$$\begin{cases} 0 < \bar{x}_3^\star(\eta_h) < b \\ -\gamma\bar{x}_1^\star(\eta_h) \leq \bar{x}_2^\star(\eta_h) \leq \gamma\bar{x}_1^\star(\eta_h) \\ \bar{x}_1^\star(\eta_h) > 0 \end{cases}. \tag{27}$$
3) $\bar{\boldsymbol{x}}^\star(\beta_h) = [\tilde{\boldsymbol{q}}^\star(\beta_h)^T, b]^T$ with
$$\tilde{\boldsymbol{q}}^\star(\beta_h) = \left(\tilde{\boldsymbol{A}}_1^T\tilde{\boldsymbol{A}}_1 + \beta_h\boldsymbol{I}\right)^{-1}\tilde{\boldsymbol{A}}_1^T\left(\boldsymbol{g} - \tilde{\boldsymbol{a}}_3 b\right),$$
where $\tilde{\boldsymbol{A}} = \left[\tilde{\boldsymbol{A}}_1, \tilde{\boldsymbol{a}}_3\right]$ and β_h, $h = 1,\ldots,N_{r_1}$ ($N_{r_1} \leq 4$) are the roots of the fourth order equation
$$\tilde{\boldsymbol{q}}^\star(\beta)^T\tilde{\boldsymbol{q}}^\star(\beta) = b^2 \tag{28}$$
such that
$$\begin{cases} \beta_h \geq -\lambda_{\max}\left(\tilde{\boldsymbol{A}}_1^T\tilde{\boldsymbol{A}}_1\right) - \left\{-\lambda_{\min}\left(\tilde{\boldsymbol{A}}_1^T\tilde{\boldsymbol{A}}_1\right)\right\} \\ -\gamma\tilde{q}_2^\star(\beta_h) < \tilde{q}_1^\star(\beta_h) < \gamma\tilde{q}_2^\star(\beta_h) \\ \tilde{q}_1^\star(\beta_h) > 0 \end{cases}. \tag{29}$$
4) $\bar{\boldsymbol{x}}_{4_i}^\star = \left[b/\sqrt{1+\gamma^2}, (-1)^{i+1}\gamma b/\sqrt{1+\gamma^2}, b\right]^T$, for $i = 1,2$.
5) $\bar{\boldsymbol{x}}_{5_i}^\star = \alpha_\pm^\star\left[1, (-1)^{i+1}\gamma, \sqrt{1+\gamma^2}\right]^T$, $i = 1,2$, with
$$\alpha_\pm^\star = \min\left(\max\left(0, \frac{\boldsymbol{v}_\pm^T\boldsymbol{g}}{\|\boldsymbol{v}_\pm\|^2}\right), \frac{b}{\sqrt{1+\gamma^2}}\right).$$
and $\boldsymbol{v}_\pm = \tilde{\boldsymbol{A}}\left[1, \pm\gamma, \sqrt{1+\gamma^2}\right]^T$.

Proof: See Appendix B ■

A complete summary of the global optimum search procedure can be found in **Algorithm 1**, in the following referred to as Angular Constrained Least Square (ACLS) method.

Some useful remarks on the devised solution technique are now in order.

Algorithm 1 Angular Constrained Least Square (ACLS) method

Input: τ_i, L_i, (x_{t_i}, y_{t_i}), $i = 1,\ldots,N$;
Output: Target location estimate $(\hat{x}_p, \hat{y}_p)$;

1) **Parameter Setup**
   - Compute the matrices $\tilde{\boldsymbol{A}}$, $\tilde{\boldsymbol{A}}_1$, and $\boldsymbol{B}$;
   - Compute the vectors $\boldsymbol{g}$, $\tilde{\boldsymbol{a}}_3$, and $\boldsymbol{v}_\pm$;
   - Compute the scalars b, γ, and $\alpha_\pm^\star$.
2) **Solutions Computation**
   - Compute $\bar{\boldsymbol{x}}_0^\star$, $\bar{\boldsymbol{x}}_{4_1}^\star$, $\bar{\boldsymbol{x}}_{4_2}^\star$, $\bar{\boldsymbol{x}}_{5_1}^\star$, and $\bar{\boldsymbol{x}}_{5_2}^\star$;
   - Find the roots $\eta_1,\ldots,\eta_{N_r}$ of the polynomial equation (25) belonging to the interval (26) and satisfying (27); then, compute $\bar{\boldsymbol{x}}^\star(\eta_i)$, $i = 1,\ldots,N_r$;
   - Find the roots $\beta_1,\ldots,\beta_{N_{r_1}}$ of the equation (28) satisfying (29); then, compute $\bar{\boldsymbol{x}}^\star(\beta_i)$, $i = 1,\ldots,N_{r_1}$;
3) **Objectives Evaluation**
   - Compute
     - $v_1 = \|\boldsymbol{g}\|^2$,
     - $v_{i+1} = \|\tilde{\boldsymbol{A}}\bar{\boldsymbol{x}}^\star(\eta_i) - \boldsymbol{g}\|^2$, $i = 1,\ldots,N_r$,
     - $v_{N_r+i} = \|\tilde{\boldsymbol{A}}\bar{\boldsymbol{x}}^\star(\beta_i) - \boldsymbol{g}\|^2$, $i = 1,\ldots,N_{r_1}$,
     - $v_{N_r+N_{r_1}+i} = \|\tilde{\boldsymbol{A}}\bar{\boldsymbol{x}}_{4_i}^\star - \boldsymbol{g}\|^2$, $i = 1,2$,
     - $v_{N_r+N_{r_1}+2+i} = \|\tilde{\boldsymbol{A}}\bar{\boldsymbol{x}}_{5_i}^\star - \boldsymbol{g}\|^2$, $i = 1,2$;
   - Determine $i^\star = \arg\min_{i\in\{1,\ldots,N_r+N_{r_1}+5\}} v_i$ and pick up the corresponding solution, i.e.,
$$\bar{\boldsymbol{x}}^\star = \begin{cases} \mathbf{0} & \text{if } i^\star = 1 \\ \bar{\boldsymbol{x}}^\star(\eta_{i^\star}) & \text{if } 2 \leq i^\star \leq N_r+1 \\ \bar{\boldsymbol{x}}^\star(\beta_{i^\star}) & \text{if } i^\star \geq N_r+2 \text{ and } i^\star \leq N_r+N_{r_1}+1 \\ \bar{\boldsymbol{x}}_{4_{i^\star}}^\star & \text{if } i^\star = N_r+N_{r_1}+2 \text{ or } i^\star = N_r+N_{r_1}+3 \\ \bar{\boldsymbol{x}}_{5_{i^\star}}^\star & \text{if } i^\star = N_r+N_{r_1}+4 \text{ or } i^\star = N_r+N_{r_1}+5 \end{cases}$$
4) **Output**
   - Set $(\hat{x}_p, \hat{y}_p) = (\bar{x}_1^\star, \bar{x}_2^\star)$.

Remark 1. ACLS method does not require any knowledge about the measurement accuracies. This is a valuable feature being such quantities dependent on the actual and, of course, unknown target position making the proposed technique effective and implementable.

Remark 2. ACLS method provides the sought position estimate in closed-form, precisely through the computation of elementary functions. In fact, the main actions in its implementation are the computation of:

A) the roots of the fourth order equations in (25) and (28);
B) $\bar{\boldsymbol{x}}^\star(\eta_i)$, $i = 1,\ldots,N_r$ and $\bar{\boldsymbol{x}}^\star(\beta_i)$, $i = 1,\ldots,N_{r_1}$;
C) $\bar{\boldsymbol{x}}_{4_1}^\star$, $\bar{\boldsymbol{x}}_{4_2}^\star$, $\bar{\boldsymbol{x}}_{5_1}^\star$, and $\bar{\boldsymbol{x}}_{5_2}^\star$;
D) the lowest objective value.

As to item A), since the eigenvalues and eigenvectors of 3×3 real matrix $\boldsymbol{B}$ can be computed in closed-form (via elementary function) resorting to [39], the equation coeffients are available in closed-form; as a result, the sought roots can be evaluated,

again in closed-form, via Cardano-Tartaglia's formula [40]. With reference to items B) and C) both the inverse of a 3×3 matrix and the considered solution points are available in closed-form. Finally item D) involves the evaluation of the objective function value for at most thirteen points and their comparison of the corresponding objectives.

IV. Other Localization Algorithms

The observation model for the 2D PBR system, i.e. Problem $\mathcal{P}$, can be expressed, without any constraints as in the following general form

$$\tilde{\boldsymbol{A}}\tilde{\boldsymbol{p}} - \boldsymbol{g} = \boldsymbol{0} \tag{30}$$

Starting from (30) and assuming $\tilde{\boldsymbol{A}}$ full-rank, different techniques can be employed to recover the unknown target position. In this paper, the following two algorithms are considered:

- LS (which is the immediate and natural extension of that proposed for the range-difference case in [37]);
- TSE [14].

A. LS Approach

The unconstrained estimator $\widehat{\tilde{\boldsymbol{p}}}_{\text{LS}}$ of $\tilde{\boldsymbol{p}}$ is given by

$$\widehat{\tilde{\boldsymbol{p}}}_{\text{LS}} = \arg\min_{\tilde{\boldsymbol{p}} \in \mathbb{R}^3} \left\{ \|\tilde{\boldsymbol{A}}\tilde{\boldsymbol{p}} - \boldsymbol{g}\|^2 \right\} = \left(\tilde{\boldsymbol{A}}^T \tilde{\boldsymbol{A}}\right)^{-1} \tilde{\boldsymbol{A}}^T \boldsymbol{g}. \tag{31}$$

B. TSE Strategy

Denoting by $\boldsymbol{\phi} = \boldsymbol{g} - \tilde{\boldsymbol{A}}\tilde{\boldsymbol{p}}$ the error vector involved in the observations model (1), the TSE strategy [14] retrieves the unknown target position assuming that $\boldsymbol{\phi}$ is a zero-mean Gaussian random vector with covariance matrix

$$\boldsymbol{\Psi} = \mathbb{E}\left[\boldsymbol{\phi}\boldsymbol{\phi}^T\right] = \boldsymbol{H}\boldsymbol{Q}\boldsymbol{H}^T, \tag{32}$$

where $\boldsymbol{H} = r\boldsymbol{I} - \textbf{diag}\left(\left[\|\tilde{\boldsymbol{p}} - \tilde{\boldsymbol{t}}_1\|, \ldots, \|\tilde{\boldsymbol{p}} - \tilde{\boldsymbol{t}}_N\|\right]\right)$. Precisely, supposing known the measurement error covariance matrix $\boldsymbol{Q}$, TSE first implements the following iterative procedure

$$\tilde{\boldsymbol{p}}_{\text{TSE}}^{(k)} = \left[\tilde{\boldsymbol{A}}^T \left(\boldsymbol{\Psi}^{(k)}\right)^{-1} \tilde{\boldsymbol{A}}\right]^{-1} \tilde{\boldsymbol{A}}^T \left(\boldsymbol{\Psi}^{(k)}\right)^{-1} \boldsymbol{g}, \quad k = 0, \ldots, K, \tag{33}$$

where K is the maximum number of iterations, $\boldsymbol{\Psi}^{(0)} = \boldsymbol{Q}$ and $\boldsymbol{\Psi}^{(k)}$, $k \geq 1$, is estimated starting from $\tilde{\boldsymbol{p}}_{\text{TSE}}^{(k-1)}$. The algorithm iteratively updates $\tilde{\boldsymbol{p}}_{\text{TSE}}^{(k)}$ until $\|\tilde{\boldsymbol{p}}_{\text{TSE}}^{(k)} - \tilde{\boldsymbol{p}}_{\text{TSE}}^{(k-1)}\| \leq \epsilon$, $k = 1, \ldots, K$, with $\epsilon > 0$, or the maximum number of iterations is reached.

The second step of TSE attempts to improve the estimation accuracy exploiting the dependency among the components of the vector $\tilde{\boldsymbol{p}}$ starting from the error vector $\boldsymbol{e}$ defined as

$$\boldsymbol{e} = \breve{\boldsymbol{p}}_{\text{TSE}} - \boldsymbol{M}\breve{\boldsymbol{p}}, \tag{34}$$

where

$$\breve{\boldsymbol{p}}_{\text{TSE}} = \left[\tilde{p}_{\text{TSE}_1}^2, \tilde{p}_{\text{TSE}_2}^2, \tilde{p}_{\text{TSE}_3}^2\right]^T, \tag{35}$$

$$\breve{\boldsymbol{p}} = \left[\tilde{p}_1^2, \tilde{p}_2^2\right]^T, \tag{36}$$

$$\boldsymbol{M} = \begin{bmatrix} 1 & 0 \\ 0 & 1 \\ 1 & 1 \end{bmatrix}, \tag{37}$$

and $\tilde{\boldsymbol{p}}_{\text{TSE}}$ is the final output of (33). Notice that, if $\boldsymbol{e} = \boldsymbol{0}$ the position of the target is directly obtained at the first step. However, errors inevitably affect $\tilde{\boldsymbol{p}}_{\text{TSE}}$ which can be modeled as

$$\tilde{\boldsymbol{p}}_{\text{TSE}} = \tilde{\boldsymbol{p}} + \boldsymbol{n}, \tag{38}$$

where $\boldsymbol{n} = [n_1, n_2, n_3]^T$ are the estimation errors at the first step. Substituting (38) in (34) and ignoring the terms n_1^2, n_2^2, n_3^2, the covariance matrix of the error vector $\boldsymbol{e}$ can be approximated as [14]

$$\boldsymbol{\Omega} = \mathbb{E}\left[\boldsymbol{e}\boldsymbol{e}^T\right] \approx 4\boldsymbol{D}\boldsymbol{F}\boldsymbol{D}, \tag{39}$$

where $\boldsymbol{D} = \textbf{diag}\left(\tilde{\boldsymbol{p}}_{\text{TSE}}\right)$ and $\boldsymbol{F}$ is an approximation for the covariance matrix of $\tilde{\boldsymbol{p}}_{\text{TSE}}$ [14] given by

$$\boldsymbol{F} \approx \left(\tilde{\boldsymbol{A}}^T \boldsymbol{\Psi}^{-1} \tilde{\boldsymbol{A}}\right)^{-1}, \tag{40}$$

with $\boldsymbol{\Psi}$ the matrix obtained evaluating (32) in correspondence of the last instance of (33). Modeling $\boldsymbol{e}$ as a Gaussian random vector, the unconstrained Maximum Likelihood Estimator (MLE) of $\breve{\boldsymbol{p}}$, obtained minimizing $\left(\breve{\boldsymbol{p}}_{\text{TSE}} - \boldsymbol{M}\breve{\boldsymbol{p}}\right)\boldsymbol{\Omega}^{-1}\left(\breve{\boldsymbol{p}}_{\text{TSE}} - \boldsymbol{M}\breve{\boldsymbol{p}}\right)$ is given by

$$\widehat{\breve{\boldsymbol{p}}} = \left(\boldsymbol{M}^T \boldsymbol{\Omega}^{-1} \boldsymbol{M}\right)^{-1} \boldsymbol{M}^T \boldsymbol{\Omega}^{-1} \breve{\boldsymbol{p}}_{\text{TSE}}. \tag{41}$$

Equation (41) provides estimates of the square value of the x and y target coordinates, respectively. Hence, the possible target locations are

$$\widehat{\tilde{\boldsymbol{p}}}_{\text{TSE},k} = \left[(-1)^k \sqrt{|\widehat{\breve{p}}_1|},\ (-1)^{(k^2+k+2)/2} \sqrt{|\widehat{\breve{p}}_2|}\right]^T, \quad k = 1, \ldots, 4. \tag{42}$$

The final estimate, chosen among the four candidates in (42), is selected as the one which gives the minimum square error χ_k, $k = 1, \ldots, 4$, defined as

$$\chi_k = \sum_{i=1}^{N} \left(\|\widehat{\tilde{\boldsymbol{p}}}_{\text{TSE},k}\| + \|\tilde{\boldsymbol{t}}_i - \widehat{\tilde{\boldsymbol{p}}}_{\text{TSE},k}\| - L_i - c\tau_i\right)^2, \quad k = 1, \ldots, 4, \tag{43}$$

with $\tilde{\boldsymbol{t}}_i = \boldsymbol{U}^T[x_{t_i}, y_{t_i}]^T$, $i = 1, \ldots, N$, the locations of the transmitters of opportunity in the rotated reference system.

V. Performance Analysis

This section is devoted to the performance assessment of the proposed target localization algorithm for a PBR exploiting multiple transmitters of opportunity. As case study, a localization scenario comprising $N = 3$ omni-directional broadcast transmitters of opportunity is analyzed. As to the specific geometric configuration, the transmitters are located at the

vertices of an equilateral triangle whose barycenter is the position of the receiver, that coincides with the origin of the reference system. Precisely, the distance of each transmitter of opportunity from the receiver is $L_i = 10$ km, $i = 1, 2, 3$. The considered setup is graphically illustrated in Figure 4.

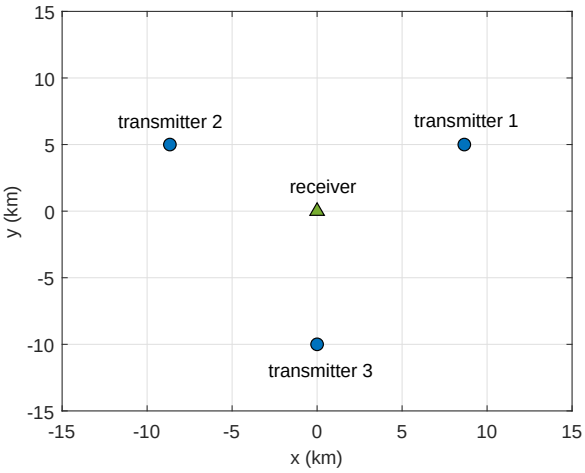

Fig. 4. Geometric configuration composed of a receiver at the reference system origin and $N = 3$ transmitters of opportunity located at the vertices of an equilateral triangle ($L_i = 10$ km, $i = 1, 2, 3$).

Modelling the measurement errors according to (3), the SNR of the $N = 3$ bistatic pairs (receiver-transmitter of opportunity) is set as [36]

$$\text{SNR}_i = \text{SNR}_0 \frac{\|\boldsymbol{q}_0\|^2}{\|\boldsymbol{p}\|^2} \frac{\|\boldsymbol{q}_0 - \boldsymbol{t}_1\|^2}{\|\boldsymbol{p} - \boldsymbol{t}_i\|^2}, \quad i = 1, 2, 3, \tag{44}$$

where $\boldsymbol{t}_i = [x_{t_i}, y_{t_i}]^T$, $i = 1, 2, 3$, are the locations of the transmitters of opportunity, $\boldsymbol{p}$ is the true target position, and SNR_0 is a reference SNR value computed via the bistatic radar range equation [18], [36] related to a reference point $\boldsymbol{q}_0 = [\bar{x}, \bar{y}]^T$ and considering the transmitter located at $\boldsymbol{t}_1$ as radiation source.

The performance of the devised localization algorithm is assessed considering as figure of merit the Root Mean Square Error (RMSE) of the target position estimate. To this end, due to the lack of a closed-form expression for the RMSE, Monte Carlo simulation method is employed, performing 1000 independent runs. The analyses are conducted also in comparison with the LS and TSE algorithms described in Section IV, and with the Root CRLB (RCRLB) benchmark, i.e. $\sqrt{\text{tr}\left(\text{FIM}^{-1}\right)}$ with FIM the Fisher Information Matrix, which is reported for completeness in Appendix C.

The first study considers a target located at $(x_p, y_p) = (r\cos\theta_p, r\sin\theta_p)$ with $r = 40$ km and different values of θ_p, $\theta_p = -9, -7, 0, 7, 9$ deg as illustrated in Figure 5(a). Moreover, the receiving antenna is assumed steered at $\theta = 0$ deg with a main-beam width of $\bar{\theta} = 10$ deg.

The obtained results are reported in Figure 6, where the RMSE is plotted versus SNR_0 for $B_i = 150$ kHz (representative of FM radio stations), $i = 1, 2, 3$. Therein, SNR_0 coincides with the actual SNR, regardless of the target position. Indeed, it is assumed that the reference point $\boldsymbol{q}_0$ involved in the SNR computation coincides with the actual target position $\boldsymbol{p}$, therefore $\boldsymbol{q}_0$ changes among the subplots.

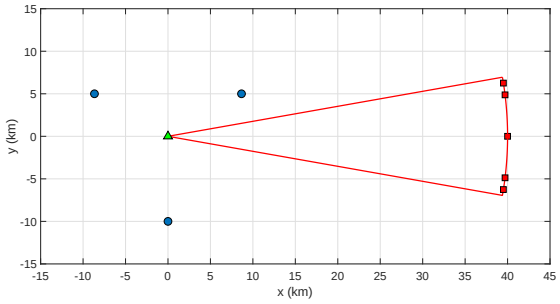

(a) Scenario 1.

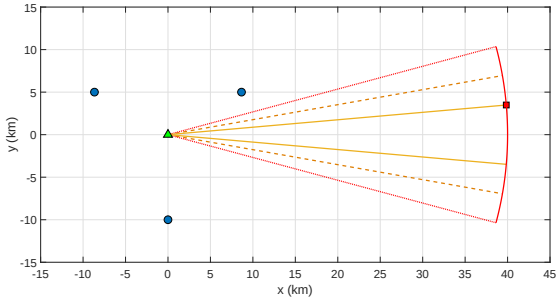

(b) Scenario 2.

Fig. 5. Simulation scenarios considered to evaluate the performance of the proposed ACLS algorithm ($r = 40$ km).

The curves show that for low SNR values, the ACLS provides better performance than the unconstrained LS and TSE counterparts, clearly revealing the effectiveness of the new procedure to exploit a-priori information on the beampattern main-beam size[3]. Specifically, the RMSE values achieved by ACLS are close to the RCRLB and for very low SNR values also lower than the limit bound (this last behavior does not represent an inconsistency and has a precise theoretical justification. In fact, when the SNR is low, our estimator becomes biased and the corresponding RMSE is not precluded to be smaller than the RCRLB which represents the limiting performance for unbiased estimators). Interestingly, as the SNR increases, all the considered positioning algorithms, i.e., ACLS, unconstrained LS, and TSE, improve their location estimation performance providing RMSE values converging to the RCRLB benchmark. Finally, it is worth observing that the closer the target position to the main-lobe boundary the better the performance of the ACLS method as compared with the counterparts. This is not surprising since the a-priori information on the beampattern extent becomes more and more valuable when the target lies in proximity of the boundary region. Indeed, in such condition even small measurement errors on the bistatic ranges might lead the target position estimate outside the feasible space region (i.e. main-beam) with a resulting high estimation error.

[3]Comparison between the curves of the ACLS and standard LS allows to quantify directly the performance benefits arising from the use of prior information.

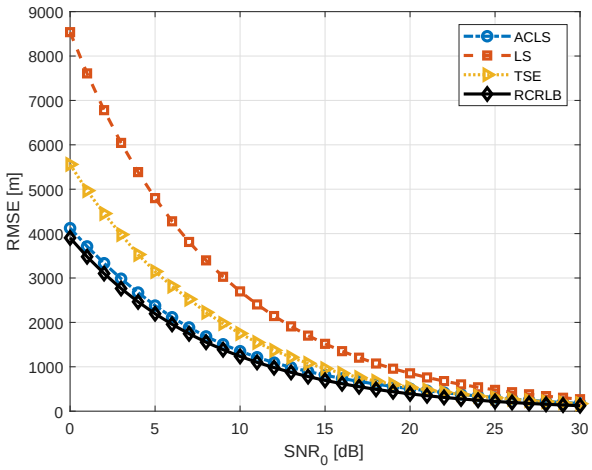

(a) $\theta_p = -9°$.

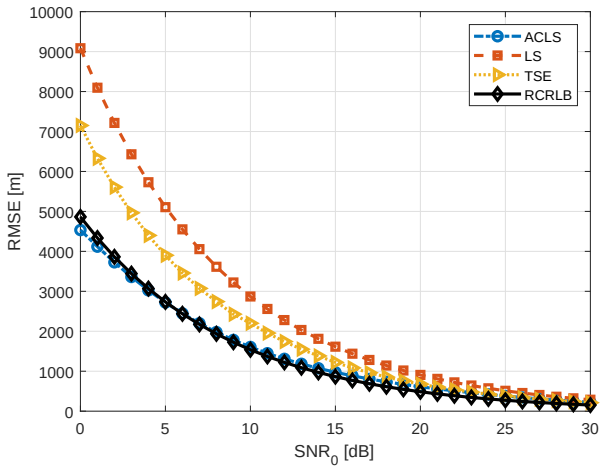

(b) $\theta_p = 9°$.

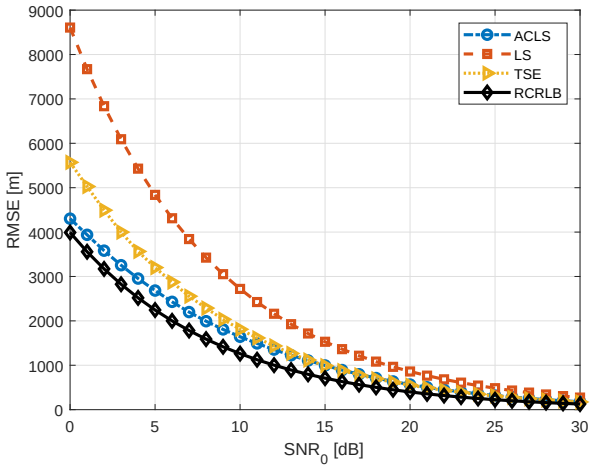

(c) $\theta_p = -7°$.

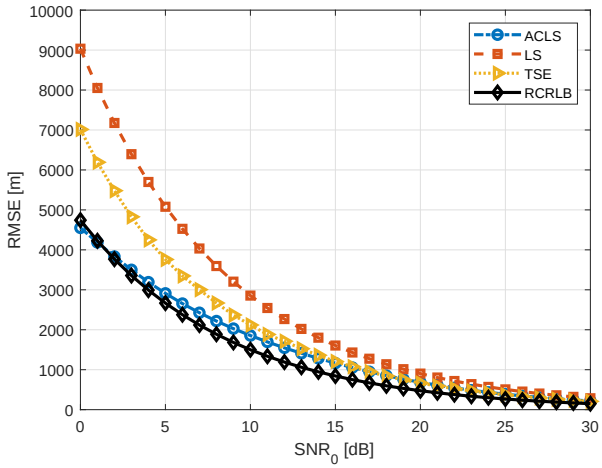

(d) $\theta_p = 7°$.

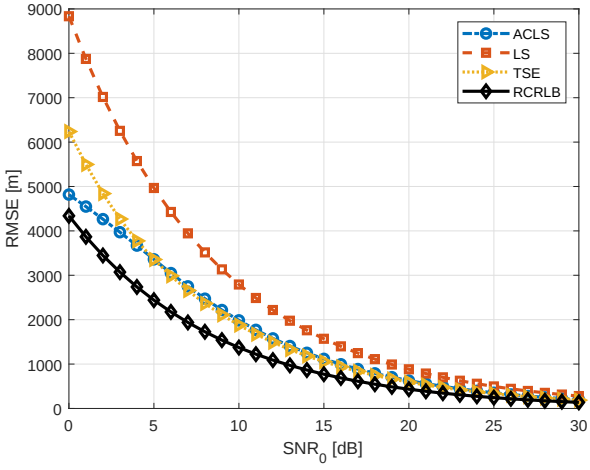

(e) $\theta_p = 0°$.

Fig. 6. RMSE versus SNR_0 assuming $\boldsymbol{p} = \boldsymbol{q}_0$ for scenario 1 of Figure 5 considering $B_i = 150$ kHz, $i = 1, 2, 3$.

To corroborate previous insights, in Figure 7 the RMSE of ACLS, unconstrained LS, and TSE, assuming the sensor configuration depicted in Figure 5(b), is reported. Precisely, this simulated scenario refers to a fixed target location, i.e., $(x_p, y_p) = (r\cos\theta_p, r\sin\theta_p)$ with $r = 40$ km and $\theta_p = 5$ deg, varying the receiving antenna beamwidth, i.e., $\bar{\theta} = 5, 10, 15$

deg. Again, the receiving antenna boresight is $\theta = 0$ deg. The results highlight that the ACLS method experiences a performance loss as the main-beam width increases, reflecting the reduced effectiveness of the forced beampattern constraint. Finally, before concluding this sub-section, it is explicitly mentioned that some additional analyses, using different number of transmitters, have confirmed the reported performance behavior.

A. Illustrative Example on the Behavior of Algorithm 1

To shed light on **Algorithm 1** working principles, in this subsection the behavior of Problem $\mathcal{P}$ objective function is sketched. In addition, the location and objective value of the candidate solutions provided by Algorithm 1 are also illustrated. To this end, the simulation setup of scenario 2 in Figure 5 with $\text{SNR}_0 = 15$ dB ($\boldsymbol{q}_0 = \boldsymbol{p}$) and $B_i = 150$ kHz, $i = 1, 2, 3$, is considered. Moreover, the target is located at $\theta_p = 5$ deg and $r = 40$ km. As to the receiver, the antenna boresight is at $\theta = 0$ deg and a beamwidth of $\bar{\theta} = 10$ deg is assumed.

In Figure 8 the isolines of the objective function, for a specific Monte Carlo trial, i.e., $\tau_1 = 0.20432$ ms, $\tau_2 = 0.26028$ ms, and $\tau_3 = 0.24157$ ms are reported. Besides, in the same figure, all the candidate optimal solutions computed by Algorithm 1 are shown[4]. Among them the optimal one is displayed with a black diamond.

Furthermore, the red square localizes the true target position, i.e., $(39.8478, 3.4862)$ km, whereas dot-dashed red lines refer to the receiving antenna main-lobe. Finally, the dotted black line defines the circle of radius b where the target position estimate must reside. Inspection of Figure 8(a) proves that the ACLS method actually selects as optimal solution that ensuring the lowest value of the objective function; this is better illustrated in subplot b) where a zoom around the optimal solution is shown.

VI. Conclusions

In this paper an innovative approach for the elliptic location has been proposed with reference to a PBR receiver that exploits multiple transmitters of opportunity. To this end, at the design development, some constraints have been enforced to the target localization process in order to exploit a-priori information on the receiving antenna main-beam size. Therefore, the problem has been formulated as a constrained LS estimation whose optimal solution provides the Cartesian coordinates of the target. To handle the resulting non-convex optimization problem, an efficient solution technique able to provide a global optimal point has been developed. In addition, it has been shown that the sought estimate belongs to a finite set, with cardinality at most thirteen, of feasible points obtainable in closed-form via elementary functions.

The conducted analyses have demonstrated the effectiveness of the proposed algorithm also in comparison with other counterparts available in the open literature especially for low SNRs. Precisely, for the considered study cases, the curves have highlighted that the RMSE values attained by the novel

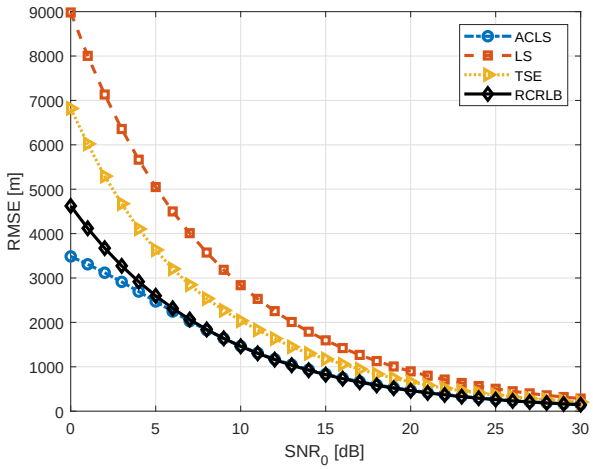

(a) $\bar{\theta} = 5°$.

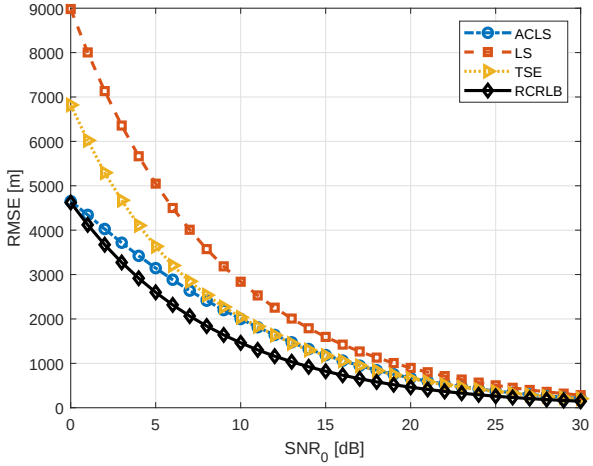

(b) $\bar{\theta} = 10°$.

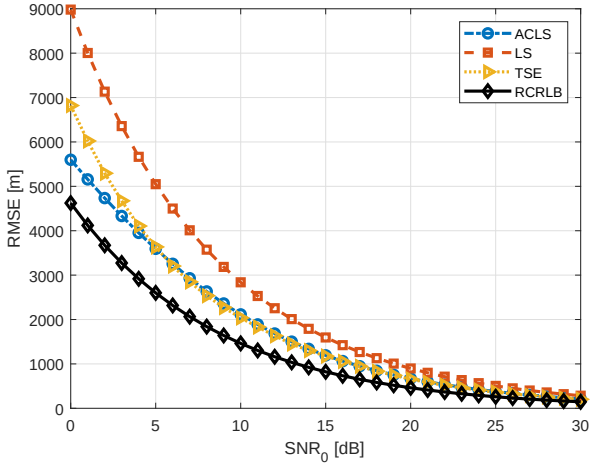

(c) $\bar{\theta} = 15°$.

Fig. 7. RMSE versus SNR_0 assuming $\boldsymbol{p} = \boldsymbol{q}$ for scenario 2 of Figure 5 considering $B_i = 150$ kHz, $i = 1, 2, 3$.

[4]The candidate solutions provided by Algorithm 1 in this specific trial are given by $\bar{\boldsymbol{x}}^\star = (0, 0)$ km, $\bar{\boldsymbol{x}}^\star(\eta) = (39.5384, 4.9360)$ km, $\bar{\boldsymbol{x}}^\star_{4_1} = (70.0351, 12.3491)$ km, $\bar{\boldsymbol{x}}^\star_{4_2} = (70.0351, -12.3491)$ km, $\bar{\boldsymbol{x}}^\star_{5_1} = (39.2392, 6.9189)$ km, $\bar{\boldsymbol{x}}^\star_{5_2} = (39.2392, -6.9189)$ km.

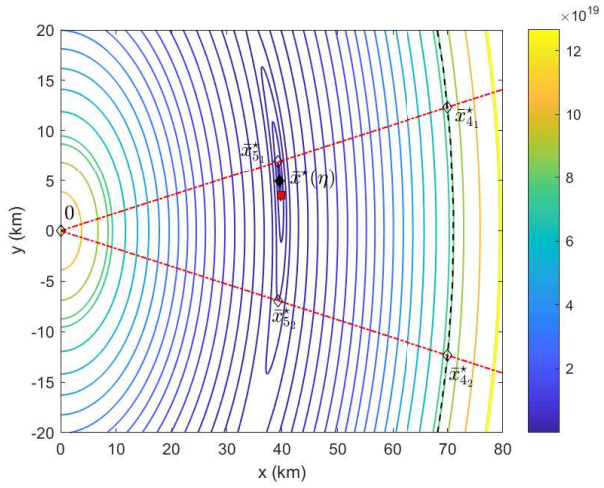

(a) objective function isolines

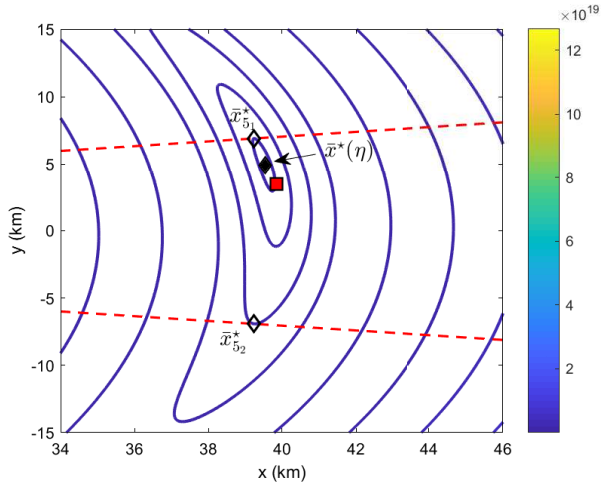

(b) zoomed part

Fig. 8. Isolines of the objective function assuming $\boldsymbol{p} = \boldsymbol{q}$, for $\mathrm{SNR}_0 = 15$ dB, $B_i = 150$ kHz, $i = 1, 2, 3$, $\theta = 0$ deg, $\bar{\theta} = 10$ deg, and $\theta_p = 5$ deg. Subplots refer to either the entire considered scenario or a zoomed part. The symbols are: ◊-marker possible solutions of ACLS, ♦-marker selected solution of ACLS, □-marker true target position.

technique are usually lower than those of the competitors, therefore validating the benefits provided by the additional constraints on the receiving antenna main-lobe extent. As a matter of fact, the obtained results have shown values very close to those of theoretical CRLB.

Future research developments might concern the test of the proposed algorithm on real recorded PBR data as well as a theoretical statistical analysis of its performance.

APPENDIX

A. Proof of Lemma 3.1

Let $\bar{\boldsymbol{x}}$ be a feasible point for $\mathcal{P}$. If $\bar{x}_1 = 0$ or $\bar{x}_3 = 0$, then all the constraints (24a)-(24d) are active and $\bar{\boldsymbol{x}} = [0, 0, 0]^T$ is the only feasible point. Hence, let us focus on $\bar{x}_1 > 0$ and $\bar{x}_3 > 0$, i.e., the inequality constraint on the left of (24b) as well as the constraint (24d) are inactive. To study the regularity of $\bar{\boldsymbol{x}}$, the following cases should be distinguished:

1) constraints (24b) and (24c) are inactive. The gradient
$$\nabla\tilde{\boldsymbol{p}}^T\boldsymbol{B}\tilde{\boldsymbol{p}}\big|_{\tilde{\boldsymbol{p}}=\bar{\boldsymbol{x}}} = 2[\bar{x}_1, \bar{x}_2, -\bar{x}_3]^T \neq 0$$
implying the regularity of $\bar{\boldsymbol{x}}$.
2) $\bar{x}_3 = b$ and constraints (24c) are inactive. The gradients
$$\nabla\tilde{\boldsymbol{p}}^T\boldsymbol{B}\tilde{\boldsymbol{p}}\big|_{\tilde{\boldsymbol{p}}=\bar{\boldsymbol{x}}} = 2[\bar{x}_1, \bar{x}_2, -b]^T$$
and
$$\nabla\tilde{p}_1 = [1, 0, 0]^T$$
are linearly independent and hence $\bar{\boldsymbol{x}}$ is regular.
3) $\bar{x}_3 = b$ and $\bar{x}_2 = \bar{x}_1\gamma$ (or $\bar{x}_2 = -\bar{x}_1\gamma$). The gradients
$$\nabla\tilde{\boldsymbol{p}}^T\boldsymbol{B}\tilde{\boldsymbol{p}}\big|_{\tilde{\boldsymbol{p}}=\bar{\boldsymbol{x}}} = 2[\bar{x}_1, \gamma\bar{x}_1, -b]^T$$
$$(\text{or } \nabla\tilde{\boldsymbol{p}}^T\boldsymbol{B}\tilde{\boldsymbol{p}}\big|_{\tilde{\boldsymbol{p}}=\bar{\boldsymbol{x}}} = 2[\bar{x}_1, -\gamma\bar{x}_1, -b]^T),$$
$$\nabla\tilde{p}_3 = [0, 0, 1]^T,$$
and
$$\nabla\left(\tilde{p}_2 - \tilde{p}_1\gamma\right) = [-\gamma, 1, 0]^T$$
$$(\text{or } \nabla\left(-\tilde{p}_2 - \tilde{p}_1\gamma\right) = [-\gamma, -1, 0]^T)$$
are linearly independent implying the regularity of $\bar{\boldsymbol{x}}$.
4) $\bar{x}_2 = \bar{x}_1\gamma$ (or $\bar{x}_2 = -\bar{x}_1\gamma$) and (24b) are inactive. The gradients
$$\nabla\tilde{\boldsymbol{p}}^T\boldsymbol{B}\tilde{\boldsymbol{p}}\big|_{\tilde{\boldsymbol{p}}=\bar{\boldsymbol{x}}} = 2[\bar{x}_1, \gamma\bar{x}_1, -\bar{x}_3]^T$$
$$(\text{or } \nabla\tilde{\boldsymbol{p}}^T\boldsymbol{B}\tilde{\boldsymbol{p}}\big|_{\tilde{\boldsymbol{p}}=\bar{\boldsymbol{x}}} = 2[\bar{x}_1, -\gamma\bar{x}_1, -\bar{x}_3]^T)$$
and
$$\nabla\left(\tilde{p}_2 - \tilde{p}_1\gamma\right) = [-\gamma, 1, 0]^T$$
$$(\text{or } \nabla\left(-\tilde{p}_2 - \tilde{p}_1\gamma\right) = [-\gamma, -1, 0]^T)$$
are linearly independent and hence $\boldsymbol{x}$ is regular.

B. Proof of Proposition 3.2

Since the objective function is continuous and the constraint set is compact, Weierstrass theorem ensures that a global minimizer exists. Let us now observe that if $\tilde{p}_1 = 0$ and/or $\tilde{p}_3 = 0$, the only feasible solution to $\mathcal{P}$ is $\bar{\boldsymbol{x}} = [0, 0, 0]^T$. Thus, in the following we focus on $\tilde{p}_1 > 0$ and $\tilde{p}_3 > 0$. Before proceeding further, it is worth pointing out that the main idea of the subsequent proof is to determine candidate optimal solutions seeking within the subsets defined by specific problem constraints. To this end, different cases, accounting for different portions of the feasible set, are analyzed in the following:

a) Assume all the inequality constraints inactive, candidate optimal points to $\mathcal{P}$ can be found among the regular points of
$$\mathcal{P}_1 \begin{cases} \min\limits_{\tilde{\boldsymbol{p}}} & \left\|\tilde{\boldsymbol{A}}\tilde{\boldsymbol{p}} - \boldsymbol{g}\right\|^2 \\ \text{s.t.} & \tilde{\boldsymbol{p}}^T\boldsymbol{B}\tilde{\boldsymbol{p}} = 0 \end{cases} \tag{45}$$
which satisfies the necessary optimality conditions in

[35, Theorem 3.1] and all the inequality constraints

$$\begin{cases} \tilde{p}_1 > 0 \\ 0 < \tilde{p}_3 < b \\ -\gamma\tilde{p}_1 < \tilde{p}_2 < \gamma\tilde{p}_1 \end{cases}. \tag{46}$$

In fact, if $\boldsymbol{x}^\star \neq (0,0,0)$ is an optimal point of $\mathcal{P}$, complying with (46), due to regularity, it satisfies first order and second order optimality conditions for $\mathcal{P}_1$. The regular stationary points of $\mathcal{P}_1$ complying with necessary optimality conditions can be obtained[5] as

$$\boldsymbol{x}^\star(\eta_h) = \left(\tilde{\boldsymbol{A}}^T\tilde{\boldsymbol{A}} + \eta_h\boldsymbol{B}\right)^{-1}\tilde{\boldsymbol{A}}^T\boldsymbol{g}$$

with η_h the real-valued solutions to the equation $\boldsymbol{x}^\star(\eta_h)^T\boldsymbol{B}\boldsymbol{x}^\star(\eta_h) = 0$, which belong to

$$\left(-\frac{1}{\lambda_2\left(\boldsymbol{B},\tilde{\boldsymbol{A}}^T\tilde{\boldsymbol{A}}\right)},+\infty\right) - \left\{-\frac{1}{\lambda_1\left(\boldsymbol{B},\tilde{\boldsymbol{A}}^T\tilde{\boldsymbol{A}}\right)},-\frac{1}{\lambda_3\left(\boldsymbol{B},\tilde{\boldsymbol{A}}^T\tilde{\boldsymbol{A}}\right)}\right\}. \tag{47}$$

Note that (47) is a fourth order equation in η_h and admits at most 4 real solutions which can be computed in closed-form via Cardano-Tartaglia procedure. As a consequence, for case a) there are at most four candidate points to check for optimality.

b) If $\tilde{p}_3 = b$, then $\mathcal{P}$ is equivalent to

$$\mathcal{P}_2 \begin{cases} \min\limits_{\tilde{\boldsymbol{q}}} & \left\|\tilde{\boldsymbol{A}}_1\tilde{\boldsymbol{q}} - \boldsymbol{g} + \tilde{\boldsymbol{a}}_3 b\right\|^2 \\ \text{s.t.} & \tilde{\boldsymbol{q}}^T\tilde{\boldsymbol{q}} = b^2 \\ & -\gamma\tilde{q}_1 \leq \tilde{q}_2 \leq \gamma\tilde{q}_1 \\ & \tilde{q}_1 \geq 0 \end{cases}, \tag{48}$$

where $\tilde{\boldsymbol{q}} = [\tilde{q}_1, \tilde{q}_2]^T \in \mathbb{R}^2$. Assuming $-\gamma\tilde{q}_1 < \tilde{q}_2 < \gamma\tilde{q}_1$ and $\tilde{q}_1 > 0$, candidate optimal solutions do $\mathcal{P}_2$ can be found among the feasible points of

$$\mathcal{P}_3 \begin{cases} \min\limits_{\tilde{\boldsymbol{q}}} & \left\|\tilde{\boldsymbol{A}}_1\tilde{\boldsymbol{q}} - \boldsymbol{g} + \tilde{\boldsymbol{a}}_3 b\right\|^2 \\ \text{s.t.} & \tilde{\boldsymbol{q}}^T\tilde{\boldsymbol{q}} = b^2 \end{cases}, \tag{49}$$

which comply with the necessary optimality conditions and satisfy the mentioned requirements $-\gamma\tilde{q}_1 < \tilde{q}_2 < \gamma\tilde{q}_1$ and $\tilde{q}_1 > 0$. These solutions can be obtained as

$$\tilde{\boldsymbol{q}}^\star(\beta_h) = \left(\tilde{\boldsymbol{A}}_1^T\tilde{\boldsymbol{A}}_1 + \beta_h\boldsymbol{I}\right)^{-1}\tilde{\boldsymbol{A}}_1^T(\boldsymbol{g} - \tilde{\boldsymbol{a}}_3 b) \tag{50}$$

with β_h the real-valued solutions to the fourth order equation $\tilde{\boldsymbol{q}}^{\star T}\tilde{\boldsymbol{q}}^\star = b^2$ such that $\beta_h \geq -\lambda_{\max}\left(\tilde{\boldsymbol{A}}_1^T\tilde{\boldsymbol{A}}_1\right)$, $\beta_h \neq -\lambda_{\min}\left(\tilde{\boldsymbol{A}}_1^T\tilde{\boldsymbol{A}}_1\right)$ (the case $\beta_h = -\lambda_{\min}\left(\tilde{\boldsymbol{A}}_1^T\tilde{\boldsymbol{A}}_1\right)$ can be handled following the same line of reasoning as in footnote 1). As a consequence, there are at most four candidate optimal points of $\mathcal{P}$ for case b) obtained appending to $\tilde{\boldsymbol{q}}^\star(\beta_h)$ the last component b, i.e. $[\tilde{\boldsymbol{q}}^\star(\beta_h), b]^T$.

c) $\tilde{p}_3 = b$ and $\tilde{p}_2 = \gamma\tilde{p}_1$ or $\tilde{p}_2 = -\gamma\tilde{p}_1$. There are only 2 feasible solutions to $\mathcal{P}$ which represent candidate optimal points

$$\boldsymbol{x}_{4_i}^\star = \left[\frac{b}{\sqrt{1+\gamma^2}}, (-1)^{i+1}\frac{\gamma b}{\sqrt{1+\gamma^2}}, b\right]^T,\ i = 1,2.$$

d) $\tilde{p}_2 = \gamma\tilde{p}_1$ or $\tilde{p}_2 = -\gamma\tilde{p}_1$ and the other inequality constraints are inactive. Candidate optimal solutions to $\mathcal{P}$ exhibit the form

$$\boldsymbol{x}_{5_1}^\star = \left[1,\ \gamma,\ \sqrt{1+\gamma^2}\right]^T\alpha_+^\star$$

and

$$\boldsymbol{x}_{5_2}^\star = \left[1,\ -\gamma,\ \sqrt{1+\gamma^2}\right]^T\alpha_-^\star$$

with $\alpha_+^\star$ the optimal solution to

$$\mathcal{P}_4 \begin{cases} \min\limits_{\alpha_+} & \|\boldsymbol{v}_+\alpha_+ - \boldsymbol{g}\|^2 \\ \text{s.t.} & 0 \leq \alpha_+ \leq \frac{b}{\sqrt{1+\gamma^2}} \end{cases}, \tag{51}$$

where $\boldsymbol{v}_+ = \tilde{\boldsymbol{A}}\left[1,\gamma,\sqrt{1+\gamma^2}\right]^T$, i.e.,

$$\alpha_+^\star = \min\left(\max\left(0, \frac{\boldsymbol{v}_+^T\boldsymbol{g}}{\|\boldsymbol{v}_+\|^2}\right), \frac{b}{\sqrt{1+\gamma^2}}\right), \tag{52}$$

and $\alpha_-^\star$ the optimal solution to

$$\mathcal{P}_5 \begin{cases} \min\limits_{\alpha_-} & \|\boldsymbol{v}_-\alpha_- - \boldsymbol{g}\|^2 \\ \text{s.t.} & 0 \leq \alpha_- \leq \frac{b}{\sqrt{1+\gamma^2}} \end{cases}, \tag{53}$$

where $\boldsymbol{v}_- = \tilde{\boldsymbol{A}}\left[1,-\gamma,\sqrt{1+\gamma^2}\right]^T$, i.e.,

$$\alpha_-^\star = \min\left(\max\left(0, \frac{\boldsymbol{v}_-^T\boldsymbol{g}}{\|\boldsymbol{v}_-\|^2}\right), \frac{b}{\sqrt{1+\gamma^2}}\right). \tag{54}$$

In conclusion, a global optimal point of $\mathcal{P}$ is to be searched among at most 13 candidates computed as specified in items a), b), c), and d). One ensuring the smallest objective in $\mathcal{P}$ is selected as global optimum.

C. CRLB of the Localization Problem

The unconstrained CRLB of the unknown target position vector $\boldsymbol{p} = (x,y) \in \mathbb{R}^2$, assuming the observation model (1), is given by

$$\left(\text{FIM}(\boldsymbol{p})\right)^{-1} \tag{55}$$

[5] If $\tilde{\boldsymbol{A}}^T\tilde{\boldsymbol{A}} + \eta_h\boldsymbol{B}$ is rank deficient, i.e., $\eta_h \in \left\{-\frac{1}{\lambda_1\left(\boldsymbol{B},\tilde{\boldsymbol{A}}^T\tilde{\boldsymbol{A}}\right)}, -\frac{1}{\lambda_2\left(\boldsymbol{B},\tilde{\boldsymbol{A}}^T\tilde{\boldsymbol{A}}\right)}, -\frac{1}{\lambda_3\left(\boldsymbol{B},\tilde{\boldsymbol{A}}^T\tilde{\boldsymbol{A}}\right)}\right\} = \mathcal{C}$, a different solution technique is required to solve the Karush-Kuhn-Tucker (KKT) equations. Precisely (assuming $\lambda_1\left(\boldsymbol{B},\tilde{\boldsymbol{A}}^T\tilde{\boldsymbol{A}}\right) \neq \lambda_2\left(\boldsymbol{B},\tilde{\boldsymbol{A}}^T\tilde{\boldsymbol{A}}\right) \neq \lambda_3\left(\boldsymbol{B},\tilde{\boldsymbol{A}}^T\tilde{\boldsymbol{A}}\right)$), let $\bar{\eta}_h \in \mathcal{C}$, $\boldsymbol{p}^\star = \left(\tilde{\boldsymbol{A}}^T\tilde{\boldsymbol{A}} + \bar{\eta}_h\boldsymbol{B}\right)^\dagger\tilde{\boldsymbol{A}}^T\boldsymbol{g}$ a solution to the (assumed solvable) linear equations system $\left(\tilde{\boldsymbol{A}}^T\tilde{\boldsymbol{A}} + \bar{\eta}_h\boldsymbol{B}\right)\boldsymbol{p} = \tilde{\boldsymbol{A}}^T\boldsymbol{g}$, and $\boldsymbol{y} \neq \boldsymbol{0}$ be a vector in the (one-dimensional) null space of $\tilde{\boldsymbol{A}}^T\tilde{\boldsymbol{A}} + \bar{\eta}_h\boldsymbol{B}$. The resulting candidate optimal solutions (for the fixed $\bar{\eta}_h$) are given by $\boldsymbol{x}^\star(\mu) = \boldsymbol{p}^\star + \nu\boldsymbol{y}$, with ν the real-valued solutions to the quadratic equation $\boldsymbol{x}^\star(\nu)^T\boldsymbol{B}\boldsymbol{x}^\star(\nu) = 0$. Remarkably, such candidate solutions are unlikely to occur practically: in more than ten thousand trials it never happens that the linear equations systems $\left(\tilde{\boldsymbol{A}}^T\tilde{\boldsymbol{A}} + \bar{\eta}_h\boldsymbol{B}\right)\boldsymbol{p} = \tilde{\boldsymbol{A}}^T\boldsymbol{g}$, $i = 1,2,3$, admit solutions.

where FIM, as already said, denotes the Fisher Information Matrix associated with the unknown parameters [41]. Note that, based on [42, Lemma 4], for the present problem the unconstrained CRLB coincides with the constrained CRLB, being $\gamma > 0$. According to the Slepian Bangs formula [14], [41], it follows that

$$\text{FIM}(\boldsymbol{p}) = \sum_{i=1}^{N} \frac{4}{c^2\sigma_i^2} \nabla h_i(\boldsymbol{p}) \left(\nabla h_i(\boldsymbol{p})\right)^T \tag{56}$$

with

$$h_i(\boldsymbol{p}) = \left(\|\boldsymbol{p}\| + \sqrt{(x - x_{t_i})^2 + (y - y_{t_i})^2} - L_i \right)$$

and

$$\begin{aligned} [\nabla h_i(\boldsymbol{p})]_1 &= \frac{\partial h_i(\boldsymbol{p})}{\partial x} \\ &= \frac{x}{\sqrt{x^2+y^2}} + \frac{x - x_{t_i}}{\sqrt{(x - x_{t_i})^2 + (y - y_{t_i})^2}} \\ [\nabla h_i(\boldsymbol{p})]_2 &= \frac{\partial h_i(\boldsymbol{p})}{\partial y} \\ &= \frac{y}{\sqrt{x^2+y^2}} + \frac{y - y_{t_i}}{\sqrt{(x - x_{t_i})^2 + (y - y_{t_i})^2}}. \end{aligned} \tag{57}$$

REFERENCES

[1] H. Kuschel, J. Heckenbach, R. Appel, et al., "Countering Stealth with Passive, Multi-Static, Low Frequency Radars," *IEEE Aerospace and Electronic Systems Magazine*, vol. 25, no. 9, pp. 11–17, 2010.

[2] M. Edrich, A. Schroeder, and F. Meyer, "Design and Performance Evaluation of a Mature FM/DAB/DVB-T Multi-Illuminator Passive Radar System," *IET Radar, Sonar & Navigation*, vol. 8, no. 2, pp. 114–122, 2014.

[3] J. Liu, H. Li, and B. Himed, "On the Performance of the Cross-Correlation Detector for Passive Radar Applications," *Signal Processing*, vol. 113, pp. 32–37, 2015.

[4] T. Higgins, T. Webster, and E. L. Mokole, "Passive Multistatic Radar Experiment Using WiMAX Signals of Opportunity. Part 1: Signal Processing," *IET Radar, Sonar & Navigation*, vol. 10, no. 2, pp. 238–247, 2016.

[5] H. D. Griffiths and C. J. Baker, *An Introduction to Passive Radar*, Artech House, 2017.

[6] R. Klemm, U. Nickel, C. Gierull, P. Lombardo, H. Griffiths, and W. Koch, Eds., *Novel Radar Techniques and Applications*, vol. 1, Scitech publishing, 2017.

[7] W. L. Melvin and J. A. Scheer, *Principles of Modern Radar: Radar Applications*, Schitech Publishing, 2014.

[8] B. T. Fang, "Simple Solutions for Hyperbolic and Related Position Fixes," *IEEE Transactions on Aerospace and Electronic Systems*, vol. 26, no. 5, pp. 748–753, September 1990.

[9] L. Rui and K. C. Ho, "Elliptic Localization: Performance Study and Optimum Receiver Placement," *IEEE Transactions on Signal Processing*, vol. 62, no. 18, pp. 4673–4688, September 2014.

[10] Junli Liang, Yuanyuan Chen, Hing-Cheung So, and Yang Jing, "Circular/Hyperbolic/Elliptic Localization via Euclidean Norm Elimination," *Signal Processing*, vol. 148, pp. 102–113, 2018.

[11] Yuan Shen, Wenhan Dai, and Moe Z. Win, "Power Optimization for Network Localization," *IEEE/ACM Transactions on Networking*, vol. 22, no. 4, pp. 1337–1350, 2013.

[12] Moe Z. Win, Yuan Shen, and Wenhan Dai, "A Theoretical Foundation of Network Localization and Navigation," *Proceedings of the IEEE*, vol. 106, no. 7, pp. 1136–1165, 2018.

[13] Moe Z. Win, Wenhan Dai, Yuan Shen, George Chrisikos, and H. Vincent Poor, "Network Operation Strategies for Efficient Localization and Navigation," *Proceedings of the IEEE*, vol. 106, no. 7, pp. 1224–1254, 2018.

[14] J. Shen, A. Molisch, and J. Salmi, "Accurate Passive Location Estimation Using TOA Measurements," *IEEE Transactions on Wireless Communications*, vol. 11, no. 6, pp. 2182–2192, June 2012.

[15] Y. Zhou, C.L. Law, Y.L. Guan, and F. Chin, "Indoor Elliptical Localization based on Asynchronous UWB Range Measurement," *IEEE Transactions on Instrumentation and Measurements*, vol. 60, no. 1, pp. 248–257, January 2011.

[16] M. Lesturgie, "Use of Dynamic Radar Signature for Multistatic Passive Localisation of Helicopter," *IEE Proceedings-Radar, Sonar and Navigation*, vol. 152, no. 6, pp. 395–403, 2005.

[17] M. Malanowski and K. Kulpa, "Two Methods for Target Localization in Multistatic Passive Radar," *IEEE transactions on Aerospace and Electronic Systems*, vol. 48, no. 1, pp. 572–580, 2012.

[18] V. Anastasio, A. Farina, F. Colone, and P. Lombardo, "Cramer - Rao Lower Bound with Pd $<$ 1 for Target Localisation Accuracy in Multistatic Passive Radar," *IET Radar, Sonar and Navigation*, vol. 8, no. 7, pp. 767–775, August 2014.

[19] E. Hanle, "Survey of Bistatic and Multistatic Radar," *Communications, Radar and Signal Processing, IEE Proceedings F*, vol. 133, no. 7, pp. 587–595, December 1986.

[20] C. Yin, S. Xu, and D. Wang, "Location Accuracy of Multistatic Radars based on Ranging Information," in *Proceedings of International Radar Conference, Beijing*, October 1996, pp. 34–38.

[21] A. Farina and E. Hanle, "Position Accuracy in Netted Monostatic and Bistatic Radar," *IEEE Transactions on Aerospace and Electronic Systems*, vol. 19, no. 4, pp. 513–520, July 1983.

[22] Y. Zhao, Y. Zhao, and C. Zhao, "A Novel Algebraic Solution for Moving Target Localization in Multi-Transmitter Multi-Receiver Passive Radar," *Signal Processing*, vol. 143, pp. 303–310, 2018.

[23] D. W. O'Hagan, H. Kuschel, M. Ummenhofer, J. Heckenbach, and J. Schell, "A Multi-Frequency Hybrid Passive Radar Concept for Medium Range Air Surveillance," *IEEE Aerospace and Electronic Systems Magazine*, vol. 27, no. 10, pp. 6–15, 2012.

[24] H. Kuschel, M. Ummenhofer, P. Lombardo, F. Colone, and C. Bongioanni, "Passive Radar Components of ARGUS 3D," *IEEE Aerospace and Electronic Systems Magazine*, vol. 29, no. 3, pp. 15–25, 2014.

[25] H. Kuschel, J. Heckenbach, and J. Schell, "Deployable Multiband Passive/Active Radar for Air Defense (DMPAR)," *IEEE Aerospace and Electronic Systems Magazine*, vol. 28, no. 9, pp. 37–45, 2013.

[26] P. E. Howland, D. Maksimiuk, and G. Reitsma, "FM Radio Based Bistatic Radar," *IEE Proceedings-Radar, Sonar and Navigation*, vol. 152, no. 3, pp. 107–115, 2005.

[27] D. K. P. Tan, H. Sun, Y. Lu, M. Lesturgie, and H. L. Chan, "Passive Radar Using Global System for Mobile Communication Signal: Theory, Implementation and Measurements," *IEE Proceedings-Radar, Sonar and Navigation*, vol. 152, no. 3, pp. 116–123, 2005.

[28] A. Farina and M. Lesturgie, "Guest Editorial: Special Issue on Bistatic and MIMO Radars and Their Applications in Surveillance and Remote Sensing," *IET Radar, Sonar & Navigation*, vol. 8, no. 2, pp. 73–74, 2014.

[29] Q. Wu, Y. D. Zhang, M. G. Amin, and B. Himed, "High-Resolution Passive SAR Imaging Exploiting Structured Bayesian Compressive Sensing," *IEEE Journal of Selected Topics in Signal Processing*, vol. 9, no. 8, pp. 1484–1497, 2015.

[30] D. Gromek, K. Kulpa, and P. Samczynski, "Experimental results of passive sar imaging using dvb-t illuminators of opportunity," *IEEE Geoscience and Remote Sensing Letters*, vol. 13, no. 8, pp. 1124–1128, Aug. 2016.

[31] P. F. Howland, "Target Tracking Using Television-Based Bistatic Radar," *IEE Proceedings-Radar, Sonar and Navigation*, vol. 146, no. 3, pp. 166–174, 1999.

[32] G. Battistelli, L. Chisci, S. Morrocchi, F. Papi, A. Farina, and A. Graziano, "Robust Multisensor Multitarget Tracker with Application to Passive Multistatic Radar Tracking," *IEEE Transactions on Aerospace and Electronic Systems*, vol. 48, no. 4, pp. 3450–3472, 2012.

[33] S. Choi, D: Crouse, P. Willett, and S. Zhou, "Multistatic Target Tracking for Passive Radar in a DAB/DVB Network: Initiation," *IEEE Transactions on Aerospace and Electronic Systems*, vol. 51, no. 3, pp. 2460–2469, 2015.

[34] More' J. J., "Generalizations of the Trust Region Subproblem," *Optim. Methods Softw.*, vol. 2, pp. 189–209, August 1993.

[35] A. Beck, P. Stoica, and J. Li, "Exact and Approximate Solutions of Source Localization Problems," *IEEE Transactions on Signal Processing*, vol. 56, no. 5, pp. 1770–1778, May 2008.

[36] M. A. Richards, J. A. Scheer, and Holm W. A., *Principles of Modern Radar: Basic Principles*, Schitech Publishing, 2010.

[37] D. J. Torrieri, "Statistical Theory of Passive Location Systems," *IEEE Transactions on Aerospace and Electronic Systems*, vol. 20, no. 2, pp. 183–198, March 1984.

[38] G. Cui, A. De Maio, A. Aubry, A. Farina, and L. Kong, "Advanced SLB Architectures with Invariant Receivers," *IEEE Transactions on Aerospace and Electronic Systems*, vol. 49, no. 2, pp. 798–818, April 2013.
[39] K. M Hasan, P. J. Basser, D. L. Parker, and A. L. Alexander, "Analytical Computation of the Eigenvalues and Eigenvectors in DT-MRI," *Journal of Magnetic Resonance*, vol. 152, no. 1, pp. 41–47, 2001.
[40] S. L. Shmakov, "A Universal Method of Solving Quartic Equations," *International Journal of Pure and Applied Mathematics*, vol. 71, no. 2, pp. 251–259, 2011.
[41] H. L. Van Trees, *Optimum Array Processing: Part IV of Detection, Estimation, and Modulation Theory*, John Wiley & Sons, 2004.
[42] J. D. Gorman and A. O. Hero, "Lower Bounds for Parametric Estimation with Constraints," *IEEE Transactions on Information Theory*, vol. 36, no. 6, pp. 1285–1301, November 1990.